SAND2022-11998C

The Optimal Control with Implicit Phase Coordination of a Collective of Wind Turbines

Joseph Young
OptimoJoe
Houston, TX
Email: joe@optimojoe.com

Wayne Weaver
Michigan Technological University
Houghton, MI
Email: wwweaver@mtu.edu

David G. Wilson
Electrical Science and Experiments
Sandia National Laboratories
Albuquerque, NM
Email: dwilso@sandia.gov

Rush D. Robinett III
Michigan Technological University
Houghton, MI
Email: rdrobine@mtu.edu

***Abstract*—The following paper details an optimal control algorithm that coordinates a small collective of wind turbines. The algorithm consists of a reduced order model (ROM) of the wind turbine collective, a discretization of the resulting state equations using a collocation method, and an optimization formulation that guides the collective's behavior. In order to validate this algorithm, the paper provides results from a scenario where two separate three turbine collectives are connected via a transmission line. Combined with energy storage, each collective delivers a constant amount of power to the grid while simultaneously coordinating their performance to bound any excessive fluctuations in the voltage. This scenario suggests that a collective of wind turbines, combined with energy storage, can be coordinated to provide a constant amount of power with consistent voltage to the grid in spite of rapidly changing wind conditions.**

***Index Terms*—Microgrid, Wind Turbine, Offshore Wind, Wind Energy, Control, Optimization**

I. Introduction

The algorithm described in the following paper is the result of an ongoing need to develop a framework to model and control power electronics formulations based on circuit components. In isolation, these models are not necessarily difficult to solve. Ultimately, these models reduce to a system of ordinary differential equations, which can be solved using a variety of known, good algorithms. Further, there exists multiple commercial software packages from companies such as MathWorks [1], Typhoon [2], and Opal-RT [3] that can quickly and efficiently model a power system.

At the same time, these packages lack the ability to generate controls that operate the power system in a constrained, optimal manner. Note, each of these properties, constrained and optimal, is important for different reasons. Optimal controls are desirable for the efficient operation of a particular system. Constrained controls are necessary to adequately model or safely operate a system. For example, an energy storage device requires a maximum capacity as well as a bound on a possible ramp rate for how quickly the device can be charged or discharged.

In pursuit of this goal, there has been steady improvement in the algorithms that optimally control these kinds of power electronics models. Wilson et al. [4] applied an optimal control approach to the operation of DC microgrids. Here, the resulting dynamics were discretized using a single step of a backward Euler discretization. This methodology was improved to multiple steps and applied to a combination of AC and DC microgrids in [5], [6]. Each of these formulations bounded the dynamics and control, but these bounds were only enforced at the discretization points. This limitation was improved by Young, Wilson, and Cook [7] when they designed the optimal control of an electric ship. There, the discretization was improved to an orthogonal spline collocation method based on Hermite cubic splines, which allowed more a more accurate solution to the system dynamics as well as bounds over the entire domain. Later, this approach was also applied to solar arrays [8] and wind turbines [9]. While effective, the use of Hermite cubic splines limits the formulation to first order DAEs and bounds on the function and its first derivative. As a result, Young, Wilson, Weaver, and Robinett [10] modified the discretization to use Bernstein polynomials, which allow for a direct discretization of a DAE of arbitrary order as well as bounds of arbitrary order.

This paper improves upon the results in [10] and [9] by focusing on a more sophisticated wind turbine control. The previous work modeled a single wind turbine collective that consisted of three turbines connected to a shared DC bus. Then, the amount of generation was maximized by extracting an arbitrary amount of power from the DC bus in order to encourage generation. The drawback to this approach is that it allows the control to use this sink like a storage device with infinite capacity in order to also moderate the voltage on the DC bus. In this paper, a constant amount of power is removed and delivered to the grid and an explicitly modeled energy storage device is added to the DC bus. This allows a better study of the amount of storage required to efficiently operate the turbines. In addition, this paper adds a second wind turbine collective connected to the first. This allows for the study of a cooperative control between multiple wind turbine collectives and whether such coordination can help limit the amount of energy storage required.

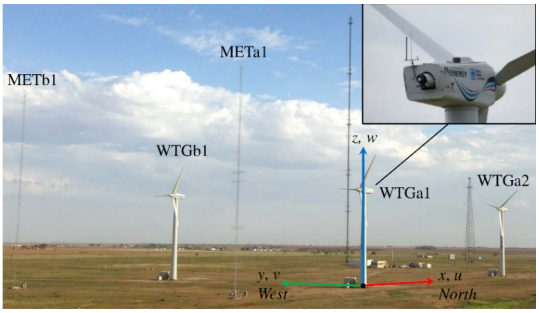

Fig. 1. Sandia Scaled Wind Farm Technology (SWiFT) facility (wind turbine pictures courtesy of Sandia SWiFT facility [11])

II. Model

The Sandia Scaled Wind Farm Technology (SWiFT) facility [11] seen in fig. 1 consists of a small collective of three wind turbines used to run experiments related to wind power generation. This presentation focuses on a reduced order model of this facility that is then cloned into a second collective, so that control and coordination between multiple collectives can be better studied. A high-level overview of the nested control architecture used to operate these collectives can be seen in fig. 2. In order to differentiate between the two, the first collective is labeled as A and the second as B. In each collective, WTGa1 and WTGb1 are well separated. In collective A, the third turbine, WTGa2, lies in the wake of WTGa1 by five rotor diameters (5D). In collective B, this turbine is offset between WTGa1 and WTGb1, so that it does not lie in the wake.

In order to model each collective, three different kinds of power system components are required and described by the circuits in figs. 3 to 5. In each of these figures, the dotted boxes represent optional components that may or may not be present due to the configuration. First, fig. 3 represents a DC bus that receives power from the wind turbines, sends a constant amount of power to the grid, and connects to other collectives in order to share energy storage and power. Here, the controlled sources i_{src} connect to and receive power from the wind turbines, i_{snk} connects to a transmission line represented by fig. 4, which ultimately connects the buses, i_P removes and sends a constant amount of power to the grid, and u represents an energy storage device connected to the bus. Next, fig. 4 models a connection between two different DC buses. The ideal transformer on the connection with voltage ratio λ enables the two different DC buses to operate at different voltages. Finally, fig. 5 models an individual wind turbine. This model largely consists of a reduced order model of a three-phase AC inductive machine run in reverse to generate rather than consume power. These three components are then interconnected according to the topology in fig. 6.

The dynamics for these models can be found in the following table. In short, the wind turbine collective is represent as a differential algebraic equation (DAE) subject to a variety of bounds that constrain the behavior of the system.

Parallel DC bus	$Cv' + \frac{v}{R} + [\sum i_p] + [\sum i_d] + [i_{obj}] + \sum i_{snk} = u + \sum \lambda i_{src}$
Non-Dispatchable load	$vi_p = P$
Dispatchable load	$vi_d = d$
Dispatchable load bound	$d \geq 0$
Voltage ratio bound	$\lambda \geq 0$
Series DC bus	$Li' + Ri + \lambda v_{snk} = u + \lambda v_{src}$
Stator d-axis	$L_s i'_{s_d} + L_m i'_{m_d} + R_s i_{s_d} - \omega_s(L_s i_{s_q} + L_m i_{m_q}) + \lambda v_{snk_d} = [u_d]$
Stator q-axis	$L_s i'_{s_q} + L_m i'_{m_q} + R_s i_{s_q} + \omega_s(L_s i_{s_d} + L_m i_{m_d}) + \lambda v_{snk_q} = [u_q]$
Rotor d-axis	$L_r i'_{r_d} - L_m i'_{r_d} + R_r i_{r_d} - (\omega_s - pN\omega_r)(L_r i_{r_q} - L_m i_{m_q}) = 0$
Rotor q-axis	$L_r i'_{r_q} - L_m i'_{r_q} + R_r i_{r_q} + (\omega_s - pN\omega_r)(L_r i_{r_d} - L_m i_{m_d}) = 0$
Slip speed bound	$\omega_s - pN\omega_r \leq 0$
Current conserv. d-axis	$i_{r_d} + i_{m_d} = i_{s_d}$
Current conserv. q-axis	$i_{r_q} + i_{m_q} = i_{s_q}$
Torque	$J\omega'_r + B\omega_r + L_m pN(i_{r_d} i_{s_q} - i_{s_d} i_{r_q}) = \tau_r$
Wind power	$\tau_r \omega_r = \frac{1}{2}\pi\rho R_m^2 v_m^3 C_m\left(\frac{R_m}{v_m}\omega_r\right)$
Parallel DC energy storage	$w' = -uv$
Series DC energy storage	$w' = -ui$
Wind energy storage	$w' = -u_d i_{s_d} - u_q i_{s_q}$
Energy storage bound	$w \geq 0$
Transformer power conserv.	$v_{snk_d} i_{s_d} + v_{snk_q} i_{s_q} = v_{dc} i_{dc}$
Transformer voltage mag.	$v_{snk_m} = v_{dc}$
AC variable mag.	$\sqrt{\gamma^2 + v_m^2} = \sqrt{\gamma^2 + \frac{2}{3}(v_d^2 + v_q^2)}$
Initial condition	$v^{(k)} = v_{k_0}$
General bound	$v_{k_{min}} \leq v^{(k)} \leq v_{k_{max}}$

In order to shape the behavior of the control, these dynamics are combined with the following objective functions

Use of storage	$\sqrt{\gamma^2 + \|w - w_{target}\|^2} - \gamma$
Parasitic losses	$\sqrt{\gamma^2 + R\|i\|^2} - \gamma$
Objective load	$-\int_0^{t_{end}} i_{obj}$
Dispatchable load shape	$\sqrt{\gamma^2 + \|d - d_{target}\|^2} - \gamma$
Dispatchable load total	$\sqrt{\gamma^2 + (\int_0^{t_{end}} d - \int_0^{t_{end}} d_{target})^2} - \gamma$

This study focuses on the objective that minimizes the use of storage. Finally, the following parameters calibrate the model to the SWiFT facility and were obtained manually

Mass moment of inertia, J	$101\,537.5\ \mathrm{kg\,m^2}$
Damping, B	$100\ \mathrm{N\,m\,s/rad}$
Pole pairs, p	2
Gearbox ratio, N	24.12
Blade length plus hub radius, R_m	13.5 m
Rotor resistance, R_r	$0.007\,645\,44\ \Omega$
Rotor inductance, L_r	$0.007\,067\,33$ H
Stator resistance, R_s	$0.009\,585\,76\ \Omega$
Stator inductance, L_s	$0.000\,252\,35$ H
Stator current d-axis, i_{s_d}	$i_{s_d} \geq 0$ A
Stator frequency, ω_s	$\omega_s \geq 0\,\mathrm{rad/s}$
Initial rotor frequency, ω_{r_0}	$2\ \mathrm{rad/s}$
Rotor frequency, ω_r	$\omega_r \in [0, 9.208]\,\mathrm{rad/s}$
Power coefficient curve, C_m	fig. 8
DC bus voltage, v	$v \in [437, 483]$ V (460 V $\pm$ 5%)
DC bus resistance, R	$1000\ \Omega$
DC bus capacitance, C	0.1 F
DC bus load (to grid), P	75 kW
Connection inductance, L	0.001 H
Connection resistance, R	$0.05\ \Omega$
Time window	600 s

Further, the model employs the additional second-order bounds, which assist in producing a smoother, more realizable control. As a note, similar behavior may be achievable using regularization.

DC bus voltage, v	$v'' \in [-20, 20]\,\mathrm{V/s^2}$

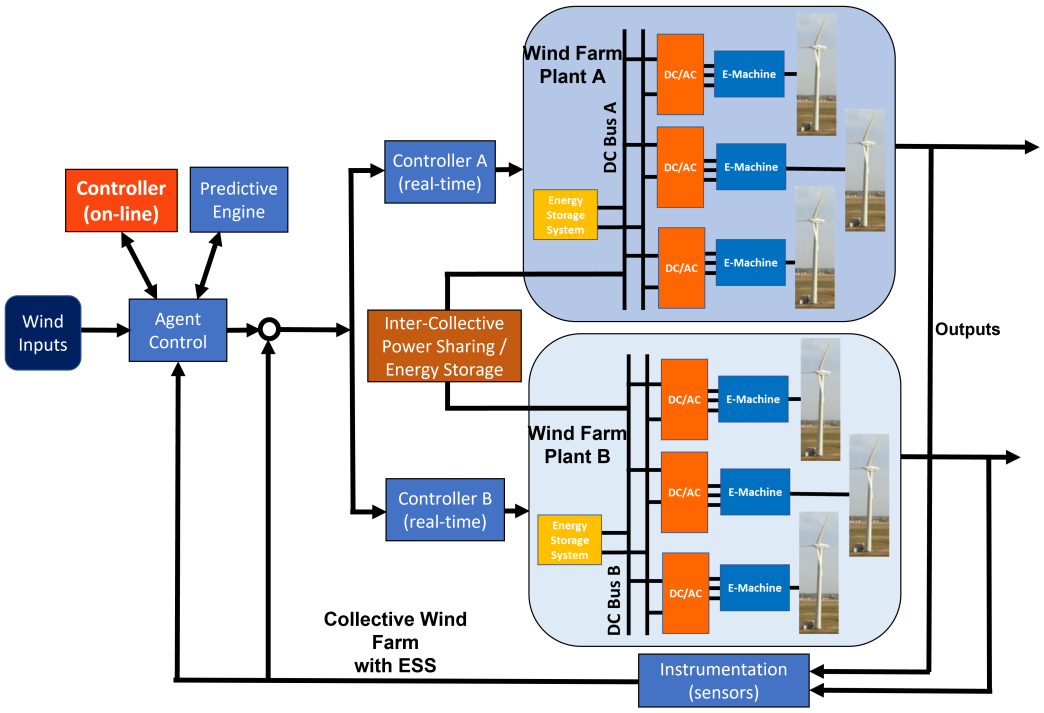

Fig. 2. Overview of the nested control architecture used to operate the collective of wind turbines

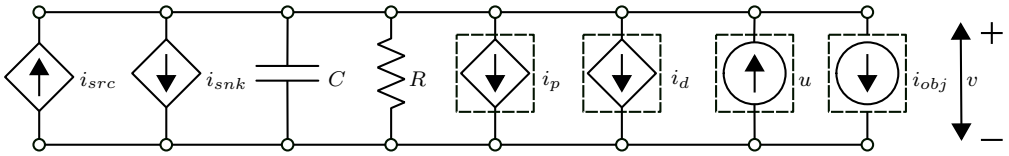

Fig. 3. Parallel DC component used to model a DC bus

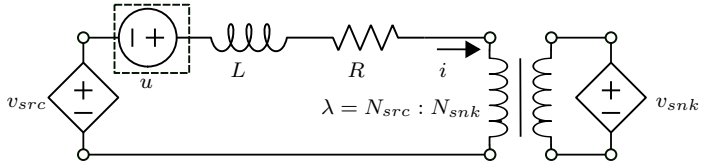

Fig. 4. Series DC component used to model a connection between two different DC buses

DC bus incom. curr., i_{src}	$i''_{src} \in [-50, 50]\,\mathrm{A/s^2}$
Objective load, i_{load}	$i''_{load} \in [-300, 300]\,\mathrm{A/s^2}$
Voltage ratio, λ	$\lambda'' \in [-1, 1]\,\mathrm{1/s^2}$
Stator current, i_s	$i''_{s_{d/q}} \in [-750, 750]\,\mathrm{A/s^2}$
Stator voltage, v_{snk}	$v''_{snk_{d/q}} \in [-1 \times 10^3, 1 \times 10^3]\,\mathrm{V/s^2}$
Stator frequency, ω_s	$\omega''_s \in [-1 \times 10^3, 1 \times 10^3]\,\mathrm{rad/s^3}$
Rotor current, i_r	$i''_{r_{d/q}} \in [-750, 750]\,\mathrm{A/s^2}$

Unless specifically denoted as a parameter, all other quantities in the above dynamics should be considered a variable in the optimization formulation. As such, this particular formulation uses a *full-space formulation* since both the control and state variables are represented and solved for explicitly in the optimization formulation.

III. Discretization

In order to discretize the equations in section II, this algorithm employs the collocation method developed by Young, Wilson, Weaver, and Robinett [10]. In short, both the state and control variables are represented as spline composed of Bernstein polynomials. Then, the dynamics are satisfied at a set of collocation points that coincide with the Chebyshev points mapped to each element in the mesh. The elements in the spline share their first and last coefficient with their neighbor, which guarantees continuity of the spline. In order words, if the spline of degree $order$ contains $nele = nmesh - 1$ elements, then the coefficients that represent the spline can be represented as a vector $c \in \mathbb{R}^{nmesh+(order-1)nele} = \mathbb{R}^{order \cdot nele+1}$. As a result, the map between the coefficients and the d-th derivative of the spline

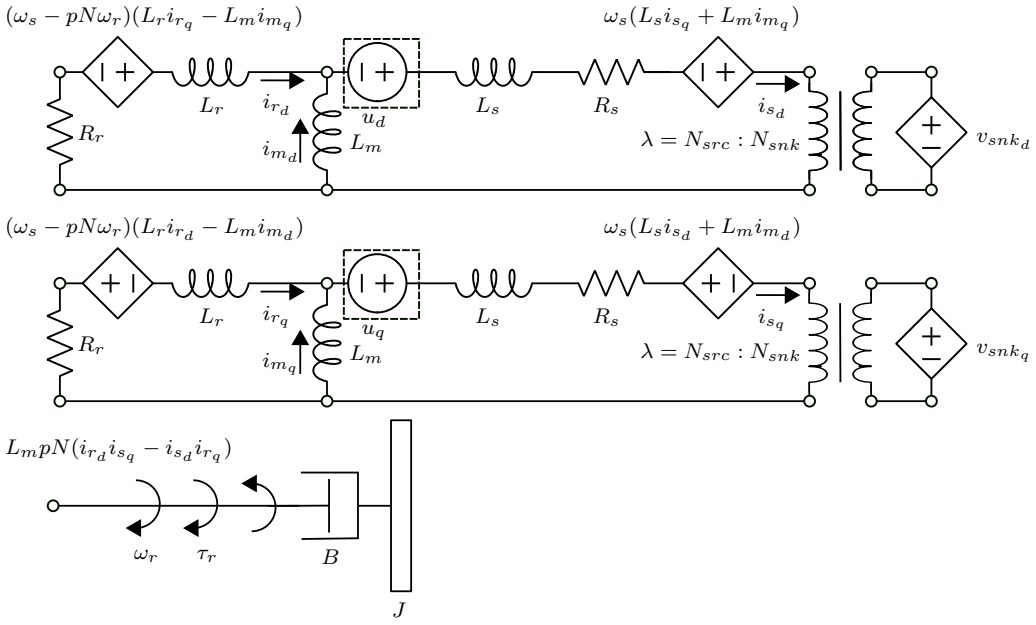

Fig. 5. Wind turbine component connected to a DC bus

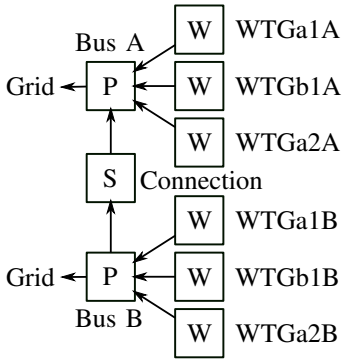

Fig. 6. Reduced order model of the SWiFT facility. P denotes a parallel DC component, S a series, and W denotes a wind turbine. Base of the arrow denotes a source and the point a sink.

evaluated at at the collocation points can be represented as a linear operator $D^{(d)} \in \mathbb{R}^{(order-d)\cdot nele+1 \times order\cdot nele+1}$.

In order to guarantee smoothness across the elements, the jump in derivative between elements is also constrained to be zero. Here, the jump means the evaluation of the spline's derivative on the left of a mesh point minus the evaluation of the spline's derivative on the right. These constraints are also linear and the jump operator of order d can be represented by the map $J^{(d)} \in \mathbb{R}^{nmesh-2 \times order\cdot nele+1}$. If the DAE has degree d, then jump operators from 1 to d are required.

Finally, any boundary conditions are imposed directly on the spline using a process similar to the derivative operators. For an ODE of degree d, this results in a boundary condition operator, $B \in \mathbb{R}^{d \times order\cdot nele+1}$.

As an example, a first-order RL circuit governed by the equation

$$\begin{aligned} &Li'(t) + Ri(t) = v(t), \\ &i(0) = i_0 \end{aligned} \tag{1}$$

can be discretized as

$$\begin{bmatrix} LD^{(1)} + RD^{(0)} \\ J^{(1)} \\ [1, 0, \ldots, 0] \end{bmatrix} c = \begin{bmatrix} v(t_{coll}) \\ 0 \\ i_0 \end{bmatrix} \tag{2}$$

where t_{coll} are the collocation points.

Beyond their use in the solution of DAEs, Bernstein polynomials possess sufficient conditions for bounding a spline. In short, since the evaluation of a Bernstein polynomial is a convex combination of its coefficients [12], bounding the coefficients of the polynomial between l and u bounds the polynomial itself between l and u. Further, since the derivative of a Bernstein polynomial is also a Bernstein polynomial, higher-order derivatives can be bounded in a similar manner. This means that a Bernstein polynomial based spline, and its derivatives, can be bounded using linear inequality constraints.

IV. Computational Results

In order to study the collective described in section II, the turbines were driven by the wind profiles in fig. 7. Recall, the configuration of collective A and B are clones of one another with the exception of the turbine WTGa2. In collective A, WTGa2 lies in the wake of WTGa1 by five rotor diameters whereas in collective B it does not. As a result, the turbines WTGa1 and WTGb1 receive the same wind profiles each collective, but the wind profile to WTGa2 differs. In both cases, the wind profiles are generated using Nalu-Wind, a generalized, unstructured, massively parallel, incompressible flow solver for wind turbine and wind farm simulations. Sprague, Anathan, Vijayakumar, and Robinson [13] provide a detailed description of the algorithm while Hsieh et al. [14] describe an application of Nalu-Wind to modeling turbines at the SWiFT facility.

In order to simulate sending power to the grid, both Bus A and Bus B contain a non-dispatchable load of 75 kW. Since the turbines themselves may not be able to always deliver

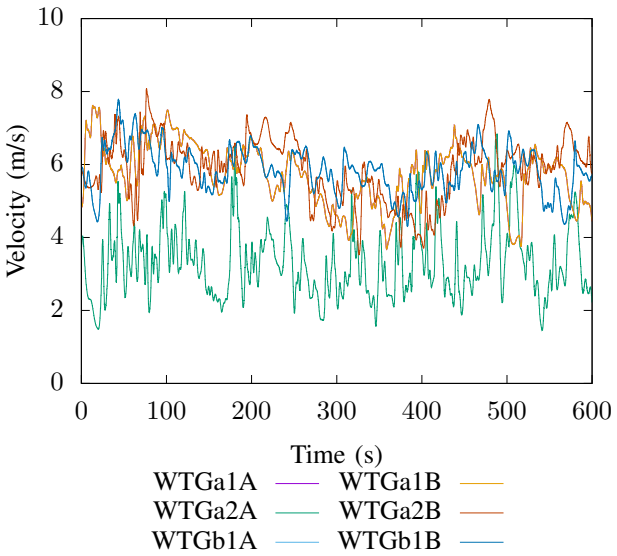

Fig. 7. Wind speed (generated from Nalu-Wind [14])

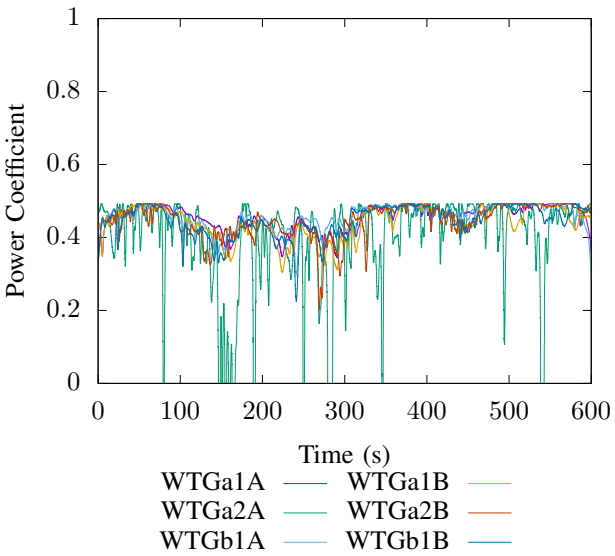

Fig. 9. Power coefficient achieved by the rotational frequency

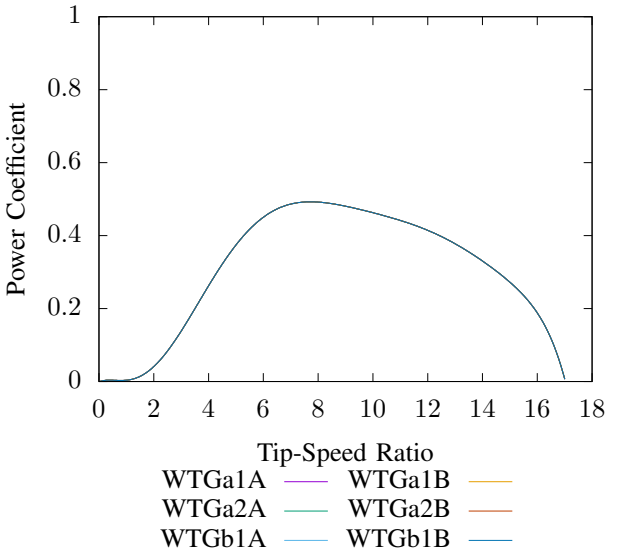

Fig. 8. Power coefficient curve

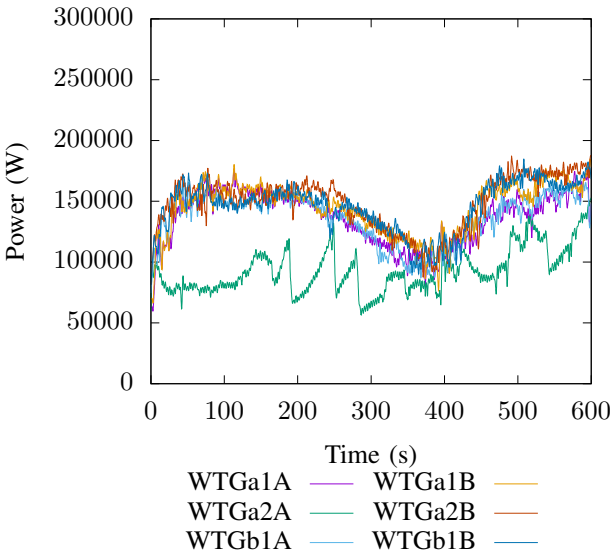

Fig. 10. Power transmitted to DC bus

this amount of power, each bus is fitted with a storage device that can store up to 10 MJ. In order to assist the the overall performance, the control attempts to keep the storage device at 80% full. This allows the storage to either deliver or store power as necessary.

As far as the optimization algorithm, the control uses a prototype version of Optizelle [15], which implements a modified version of the composite step SQP method developed by Ridzal and Heinkenschloss [16], [17], [18]. This is combined with a primal-dual interior point method in a manner similar to NITRO described by Byrd, Hribar, and Nocedal [19]. The augmented systems that arise from this formulation are solved using a rank-revealing QR factorization developed by Davis [20]. This scenario uses a formulation that contains 467 111 variables, 162 344 equality constraints, and 279 957 bounds.

In terms of the performance, the amount of generation that the turbines deliver to the DC bus can be seen in fig. 10. As should be expected, WTGa2A generates less power than the other turbines since it lies in the wake of WTGa1A. Outside of that, the amount of power delivered to the bus roughly corresponds to the wind speed in fig. 7. Next, the voltage on each DC bus is found in fig. 11. Notice that the while the voltage varies slightly, it remains close to the desired 460 V. This indicates that the control successfully coordinates the turbines and storage in order to provide a consistent voltage in the power provided to the grid. In terms of efficiency, fig. 9 shows the power coefficient achieved by each turbine on the power coefficient curve in fig. 8. This shows that each turbine operates near the maximum of the power coefficient curve with the exception of the turbine WTGa2A whose wind speed is significantly slower since it lies in the wake of

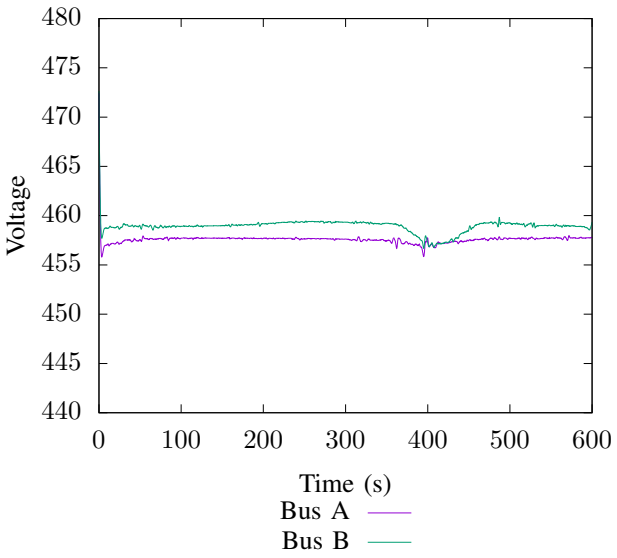

Fig. 11. Voltage on the DC bus

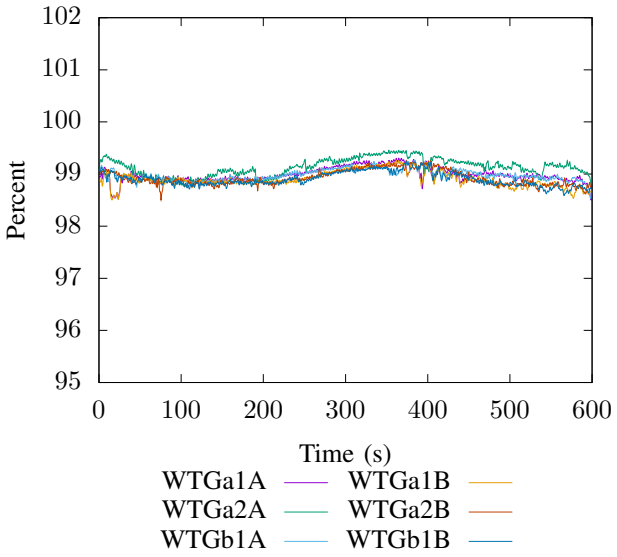

Fig. 12. Motor efficiency

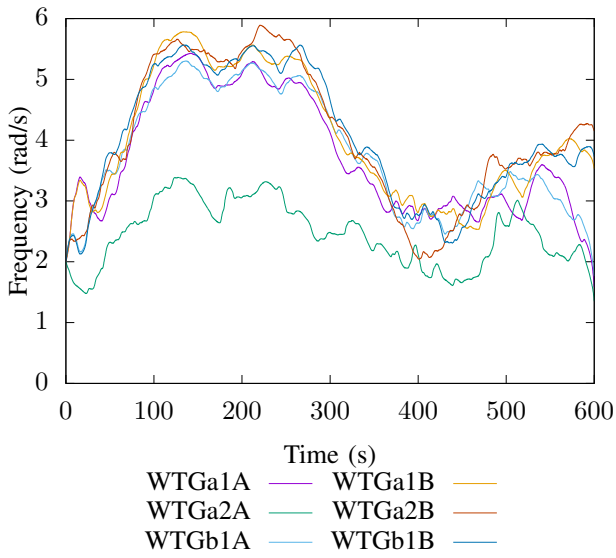

Fig. 13. Rotor frequency

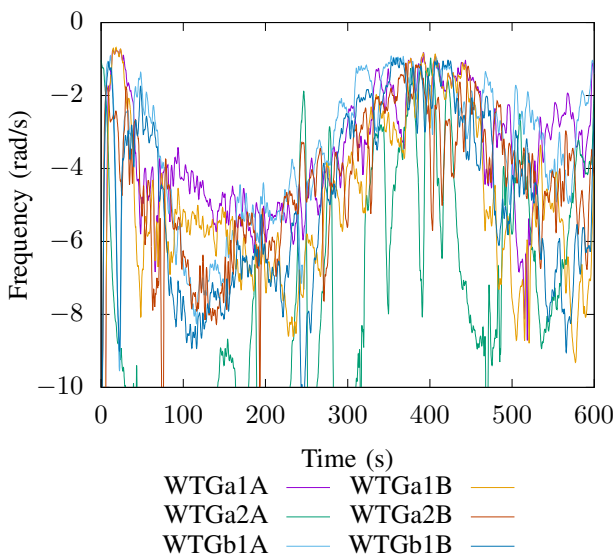

Fig. 14. Slip frequency

WTGa1A. As another metric of performance, fig. 12 displays the motor efficiency, which is defined as

$$\frac{i_{s_d} v_{snk_d} + i_{s_q} v_{snk_q} - (i_{s_d}^2 + i_{s_q}^2) R_s - (i_{r_d}^2 + i_{r_q}^2) R_r}{i_{s_d} v_{snk_d} + i_{s_q} v_{snk_q}} \quad (3)$$

This is the amount of power delivered to the DC bus, minus the parasitic losses, normalized by the amount of power delivered to the DC bus. In this scenario, the efficiency remains around 98-99%. In terms of the control, the rotor frequency can be seen in fig. 13 and the slip frequency in fig. 14. Finally, the amount of energy stored in the momentum of the turbines can be seen in fig. 15. This energy is coordinated with the amount of energy stored in the explicit energy devices seen in fig. 16, which deliver the amount of power shown in fig. 17. Although, the energy storage device can store a maximum of 10 MJ, the storage device on Bus A remains bounded between 7.67 MJ and 8.11 MJ and the storage device on Bus B remains bounded between 7.56 MJ and 8.20 MJ. This means that Bus A only requires 0.44 MJ of storage and Bus B only requires 0.63 MJ. This also demonstrates the ability of the optimal control to assist with sizing certain parameters such as energy storage.

V. Summary and Future Work

The preceding paper summarized an optimal control algorithm for the control and coordination of a small collective of wind turbines based on the Sandia SWiFT facility. The turbines and power system were modeled using a circuit based ROM. The resulting DAE was discretized using a collocation method. Then, the overall formulation was solved using an optimization solver.

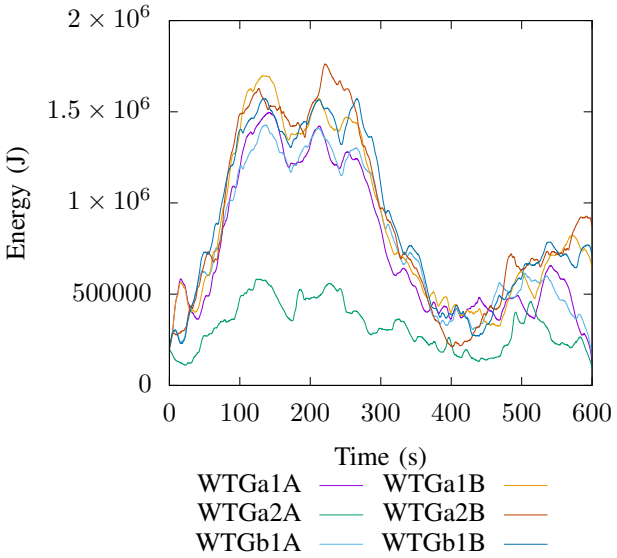

Fig. 15. Energy stored in the turbines

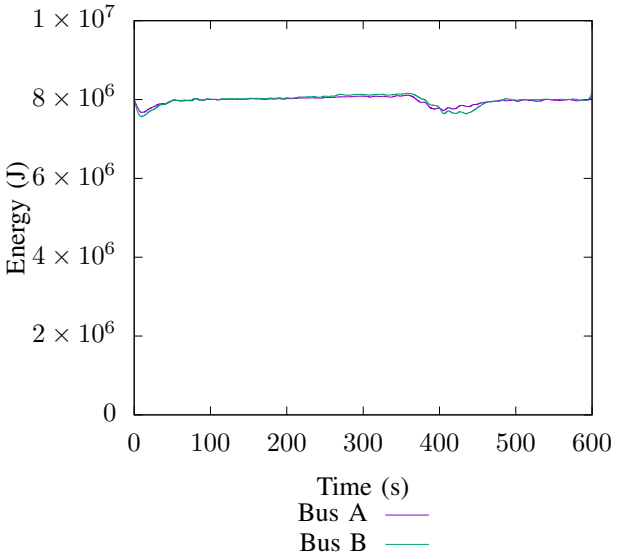

Fig. 16. Energy in the explicit storage device

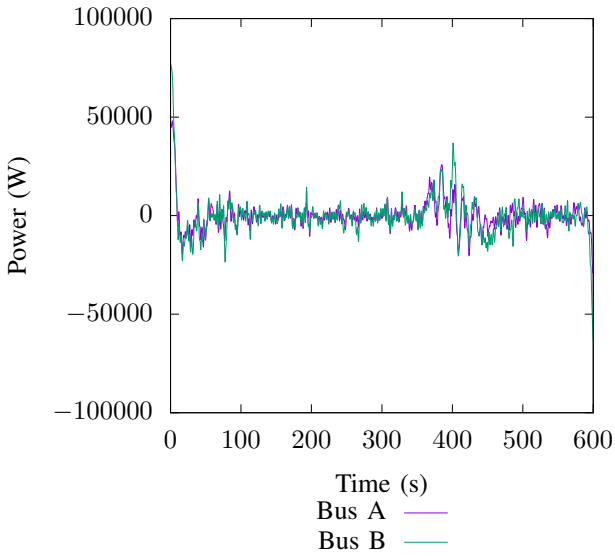

Fig. 17. Power delivered by the explicit storage device

The computational study provided encouraging results. It demonstrated that the control can successfully coordinate multiple wind turbine collectives to not only deliver a constant amount of power to the grid, but to do so at a consistent voltage. This is in spite of wildly changing wind conditions where the amount of power in the wind itself may be insufficient to generate the amount of power required by the grid. The control accomplished this by coordinating the amount of energy stored within each turbine as well as an explicit energy storage device on each bus. The simulation helped demonstrate that for this particular scenario, less than 0.63 MJ of storage was required to deliver a constant 75 kW from each wind turbine collective. As such, this kind of study can help determine the amount of energy storage required to efficiently operate a wind turbine collective.

In terms of future work, the scope, size, and design of generation can be further explored. For example, additional requirements could be added to the energy storage devices to restrict the rate that power can be stored to delivered to each bus. This could help determine the kind of energy storage device appropriate for the collectives. Alternatively, other kinds of generation could be added to the scenario such as solar or wave generators. Generally speaking, the above approach provides a framework for coordinating multiple, disparate power generation sources and delivering a constant amount of power with consistent voltage. As a result, the idea of multi-modal power generation and control can be further explored.

Acknowledgment

Sandia National Laboratories is a multimission laboratory managed and operated by National Technology and Engineering Solutions of Sandia LLC, a wholly owned subsidiary of Honeywell International Inc. for the U.S. Department of Energy's National Nuclear Security Administration under contract DE-NA0003525. This study was partially funded by the Laboratory Directed Research & Development (LDRD) program at Sandia National Laboratories. This report describes objective technical results and analysis. Any subjective views or opinions that might be expressed in the report do not necessarily represent the views of the U.S. Department of Energy or the United States Government.

This project was supported by the DOE EERE WETO Program led by our program manager Dr. Jian Fu.

Special thanks to Dr. Steve Glover and Dr. Ray Byrne at Sandia, for their technical review and programmatic leadership for this project.

References

[1] T. M. Inc., "Simulink," www.mathworks.com/products/simulink.html, 1994–2022.

[2] T. H. Inc., "Typhoon hil control center toolchain," www.typhoon-hil.com/products/hil-software/, 2022.

[3] I. Opal-RT Technologies, "Hypersim," https://www.opal-rt.com/systems-hypersim/, 2022.

[4] D. G. Wilson, J. C. Neely, M. A. Cook, S. F. Glover, J. Young, and R. D. Robinett, "Hamiltonian control design for dc microgrids with stochastic sources and loads with applications," in *2014 International Symposium on Power Electronics, Electrical Drives, Automation and Motion*, June 2014, pp. 1264–1271.

[5] D. G. Wilson, R. D. Robinett, W. W. Weaver, R. H. Byrne, and J. Young, "Nonlinear power flow control design of high penetration renewable sources for ac inverter based microgrids," in *2016 International Symposium on Power Electronics, Electrical Drives, Automation and Motion (SPEEDAM)*, June 2016, pp. 701–708.

[6] D. G. Wilson, W. Weaver, R. D. Robinett, J. Young, S. F. Glover, M. A. Cook, S. Markle, and T. J. McCoy, "Nonlinear Power Flow Control Design Methodology for Navy Electric Ship Microgrid Energy Storage Requirements," in *14th International Naval Engineering Conference & Exhibition*, 2018, pp. 1–15.

[7] J. Young, D. G. Wilson, and M. A. Cook, "The optimal control of an electric warship driven by an operational vignette," in *2021 IEEE Electric Ship Technologies Symposium (ESTS)*, 2021, pp. 1–8.

[8] J. Young, D. G. Wilson, W. Weaver, and R. D. Robinett, "Supervisory optimal control for photovoltaics connected to an electric power grid," *IET Conference Proceedings*, pp. 115–122(7), 2021.

[9] ——, "The optimal control of type-4 wind turbines connected to an electric microgrid," *IET Conference Proceedings*, pp. 283–290(7), January 2021.

[10] J. Young, D. G. Wilson, W. Weaver, and R. D. R. III, "A well-conditioned collocation method for optimal control," Submitted, 2022.

[11] "Swift facility & testing," https://energy.sandia.gov/programs/renewable-energy/wind-power/wind_plant_opt/, accessed: 2021-08-20.

[12] H. Prautzsch, W. Boehm, and M. Paluszny, *Bézier and B-Spline Techniques*. Springer, 2002.

[13] M. A. Sprague, S. Ananthan, G. Vijayakumar, and M. Robinson, "ExaWind: A multifidelity modeling and simulation environment for wind energy," *Journal of Physics: Conference Series*, vol. 1452, p. 012071, jan 2020.

[14] A. Hsieh, D. C. Maniaci, T. G. Herges, G. Geraci, D. T. Seidl, M. S. Eldred, M. L. Blaylock, and B. C. Houchens, *Multilevel Uncertainty Quantification Using CFD and OpenFAST Simulations of the SWiFT Facility*. American Institute of Aeronautics and Astronautics, Inc, 2020.

[15] J. Young, "Optizelle – an open source software library designed to solve general purpose nonlinear optimization problems," www.optimojoe.com, 2013–2022.

[16] D. Ridzal, "Trust-region SQP methods with inexact linear system solves for large-scale optimization," Ph.D. dissertation, Rice University, 2006.

[17] D. Ridzal, M. Aguiló, and M. Heinkenschloss, "Numerical study of matrix-free trust-region SQP method for equality constrained optimization," Sandia National Laboratories, Tech. Rep. SAND2011-9346, 2011.

[18] M. Heinkenschloss and D. Ridzal, "A matrix-free trust-region sqp method for equality constrained optimization," *SIAM Journal on Optimization*, vol. 24, no. 3, pp. 1507–1541, 2014.

[19] R. H. Byrd, M. E. Hribar, and J. Nocedal, "An interior point algorithm for large-scale nonlinear programming," *SIAM Journal on Optimization*, vol. 9, no. 4, pp. 877–900, 1999.

[20] T. A. Davis, "Algorithm 915, suitesparseqr: Multifrontal multithreaded rank-revealing sparse QR factorization," *ACM Trans. Math. Softw.*, vol. 38, no. 1, Dec. 2011.